J Mater Sci (2007) 42:4731–4737
DOI 10.1007/s10853-006-0825-x

X-ray diffraction, optical absorption and emission studies on Er^{3+}- and Er^{3+}/Yb^{3+}-doped Li_3NbO_4 powder

De-Long Zhang · Jia Kang · E. Y. B. Pun

Received: 15 August 2005 / Accepted: 21 August 2006 / Published online: 16 March 2007

Abstract Er^{3+}(/Yb^{3+})-doped Li_3NbO_4 powder were prepared by thermally sintering mixtures of Er_2O_3 (0.5, 1.0 mol%), Yb_2O_3 (0, 0.5, 1.0 mol%), Li_2CO_3 (48–49 mol%) and Nb_2O_5 (50 mol%) at 1125, 1150 and 1450 °C over the durations of 8–22 h. The crystalline phases contained in these samples were determined by using X-ray diffraction and discussed in comparison with a vapor-transport-equilibration-treated (VTE-treated) Er(2.0 mol%):$LiNbO_3$ single crystal and $ErNbO_4$ powder previously reported. The results show that the X-ray patterns of the rare-earth-doped samples reveal little difference each other, but large differences with those of the VTE crystal and $ErNbO_4$ powder. The doped rare-earth ions Er^{3+} (and Yb^{3+}) present in the powder as the $ErNbO_4$ (and $YbNbO_4$) phase(s). The possibility that the highly Er-doped $LiNbO_3$ crystal contains Li_3NbO_4 precipitates is small. Optical absorption and emission studies show that the only Er-doped Li_3NbO_4 powder shows similar absorption and emission characteristics with the pure $ErNbO_4$. The codopant Yb^{3+} ion enhances the 980-nm-upconversion emissions of Er^{3+} ions, results in remarkable spectral alterations at 0.98 μm region, and causes the alterations of relative absorbance and relative emission intensity of individual peaks or bands at 1.5 μm region. On the other hand, the Yb-codoping hardly affects the Er^{3+} energy structure and the lifetime of Er^{3+} ion at 1.5 μm. The measured lifetimes at 1.5 μm of Er^{3+} ions in the singly Er^{3+}- and doubly Er^{3+}/Yb^{3+}-doped mixtures have a nearly same value of ~ 1.5 ms. For the pure $ErNbO_4$ powder, the lifetime is prolonged to ~2 ms perhaps due to radiation trapping effect.

D.-L. Zhang (✉) · J. Kang
Department of Opto-electronics and Information Engineering, College of Precision Instruments and Opto-electronics Engineering, Tianjin University, Tianjin 300072, P. R. China
e-mail: delongzhang@eyou.com

D.-L. Zhang · E. Y. B. Pun
Department of Electronic Engineering, City University of Hong Kong, 83 Tat Chee Avenue, Kowloon, Hong Kong, P. R. China

Introduction

Vapor transport equilibration (VTE) technique has been proved to be a practical and effective method of altering Li/Nb ratio in a pure or doped $LiNbO_3$ or $LiTaO_3$ crystal. Recently, this technique has been applied to bulk-doped (MgO) Er(/Yb):$LiNbO_3$ [1–4]. Earlier studies have shown that when the doping level of the external dopants is less than 1.0 mol%, the VTE treatment cannot cause the precipitation of the crystal, and the VTE-treated crystal reveals several spectroscopic properties favorable for the integrated opto-electronics application besides the intrinsic merits of a pure near-stoichiometric $LiNbO_3$ crystal. On the other hand, as the doping level of the external dopants is higher than 1.0 mol%, the VTE treatment causes the precipitation of the crystal, and the originally baby-pink and transparent crystal becomes milky and opaque. Further studies have shown that the generated precipitates contain the phase $ErNbO_4$, $YbNbO_4$ and both ones in the respective case of only Er-doping, only Yb-doping and Er/Yb-codoping [3]. A detailed investigation on the crystallographic morphology and symmetry with respect to the $ErNbO_4$ precipitates [5], phonon vibration [2], crystalline phase [3–11], origin of precipitation [9], and optical absorption and emission characteristics [3, 4, 6, 7, 11, 12] has been carried out in the past few years. To understand the

precipitates, pure $ErNbO_4$ powder has been prepared by thermally sintering the mixture of Er_2O_3 and Nb_2O_5 powder according to the molar ratio 1:1 [10]. Its spectroscopic properties have been characterized by using optical absorption and photoluminescence spectroscopies [11].

On the phase diagram of the Li_2O–Nb_2O_5 system, four different compounds are present that include $3Li_2O$–Nb_2O_5 (trilithium niobate, Li_3NbO_4), Li_2O–Nb_2O_5 (lithium niobate), Li_2O–$3Nb_2O_5$ ($LiNb_3O_8$) and Li_2O–$14Nb_2O_5$ ($Li_2Nb_{28}O_{71}$) [13]. Since the VTE treatment is usually carried out at the temperature around 1100 °C in a Li-enriched atmosphere created by a mixed two-phase (Li_3NbO_4 + $LiNbO_3$) powder, there exists the possibility that the VTE treatment induces the trilithium niobate phase in a $LiNbO_3$ crystal according to the phase diagram of the Li_2O–Nb_2O_5 system. It is not sure if the above-mentioned precipitated rare-earth-doped $LiNbO_3$ crystals contain also the trilithium niobate (Li_3NbO_4) besides the $ErNbO_4$ and/or $YbNbO_4$. The first goal of present work aims at making this argument clear. Moreover, Shishido et al. [14, 15] have reported the crystal structure of the trilithium niobate grown from LiCl flux. Their studies have shown that the crystal structure of trilithium niobate (space group: $I\bar{4}3m$) has a distinct difference from that of the $ErNbO_4$ (space group: I2). Due to this difference in crystal structure, it would be interested and worthy to pay attention to the similarities and differences of the spectroscopic properties of Er^{3+} ions in the doped trilithium niobate and pure $ErNbO_4$ powder. This is another goal of present work. Towards these goals, we have prepared singly Er^{3+}-doped and Er^{3+}/Yb^{3+}-codoped trilithium niobate (Li_3NbO_4) powder by thermally sintering the mixtures of Er_2O_3 (0.5, 1.0 mol%), Yb_2O_3 (0, 0.5, 1.0 mol%), Li_2CO_3 (48–49 mol%) and Nb_2O_5 (50 mol%) at 1125, 1150 and 1450 °C over the durations of 8–22 h. Subsequently, the crystalline phases and the spectroscopic properties of Er^{3+} ions in these rare-earth-doped mixtures are investigated in comparison with the pure $ErNbO_4$ powder.

Experimental

Er_2O_3, Yb_2O_3, Li_2CO_3 and Nb_2O_5 powder, with the respective purity of 99.9%, 99.9%, 99.999% and 99.999%, were used as raw materials. The rare-earth-doped Li_2CO_3 powder was homogeneously mixed with Nb_2O_5 according to the molar ratio (Er_2O_3 + Yb_2O_3 + Li_2CO_3):Nb_2O_5 = 1:1, which corresponds to the stoichiometry of the pure Li_3NbO_4. The mixtures with the Er_2O_3/Yb_2O_3 doping levels of 0.5/0.5, 0.5/1.0, 1.0/0 and 1.0 mol%/1.0 mol% were pre-calcined at 750 °C over 6 h in a bottom loading furnace (BLF18/8) to remove the CO_2 contained in the Li_2CO_3. After fine powdering, the four mixtures were further calcined at 1450, 1150, 1150 and 1125 °C over 8, 22, 22 and 20 h, respectively.

The crystalline phases contained in these rare-earth-doped mixtures were analyzed by utilizing a Siemens D500 diffractometer equipped with a Cu target. The target voltage and current operated at 40 kV and 30 mA, respectively. The scanning range and speed of the 2θ angle are 5–90° and ~8°/min, respectively.

The absorption spectra were recorded in the wavelength range of 300–1700 nm by using a Perkin–Elmer Lambda-19 UV–VIS–NIR Spectrophotometer. The scanning step and the speed were fixed at 0.1 nm and 120 nm/min, respectively. To facilitate the optical absorption measurements, each calcined powder to be measured was diluted by KBr powder and was pressurized into a thin plate with a thickness of ~0.5 mm.

The visible fluorescence, green and red upconversion and near-infrared emission spectra of Er^{3+} ions were recorded by using a SPEX 500M monochromator equipped with a visible grating (1200 grooves/mm) and an infrared grating (600 grooves/mm) and with a photomultiplier and an InGaAs 30 TE infrared photodetector. The spectra were recorded in the ranges of 500–700, 950–1050 and 1450–1650 nm. A 980 nm laser diode with an output of 90 mW was used to excite the upconversion emissions. A 488 nm beam with an output of 150 mW, emitted from an INNOVA 400 argon laser, was used as the excitation source in the recording of the visible fluorescence and infrared emissions. The infrared emission spectra were recorded at the fixed chopper frequency of 20 Hz. The scanning step and integration time are 0.1 nm and 0.5 s, respectively. The Er^{3+} lifetime at the wavelength of 1.5 μm was measured by the aid of a digital oscilloscope (100 MHz) under the 488 nm excitation.

Results and discussions

As an example, in Fig. 1 we show X-ray diffraction pattern (see the pattern labeled by a) of a powder sample from a VTE-treated singly Er(2.0 mol%)-doped Z-cut $LiNbO_3$ single crystal with the precipitates in the bulk and on surface of the crystal. The crystal was subjected to two VTE procedures. The first VTE treatment was carried out at 1110 °C over 120 h and the second round of treatment was carried out at a relatively higher temperature 1120 °C over a relatively shorter duration of 100 hours. For convenience, in Fig. 1 we also show the diffraction pattern (pattern b) of pure $ErNbO_4$ powder, prepared by thermally sintering a mixture of Er_2O_3 (50 mol%) and Nb_2O_5 (50 mol%) powder at 1100 °C over 120 h [10]. The X-ray diffraction patterns of the singly Er^{3+}-doped and doubly Er^{3+}/Yb^{3+}-doped mixtures are shown in upper part of Fig. 1 and are

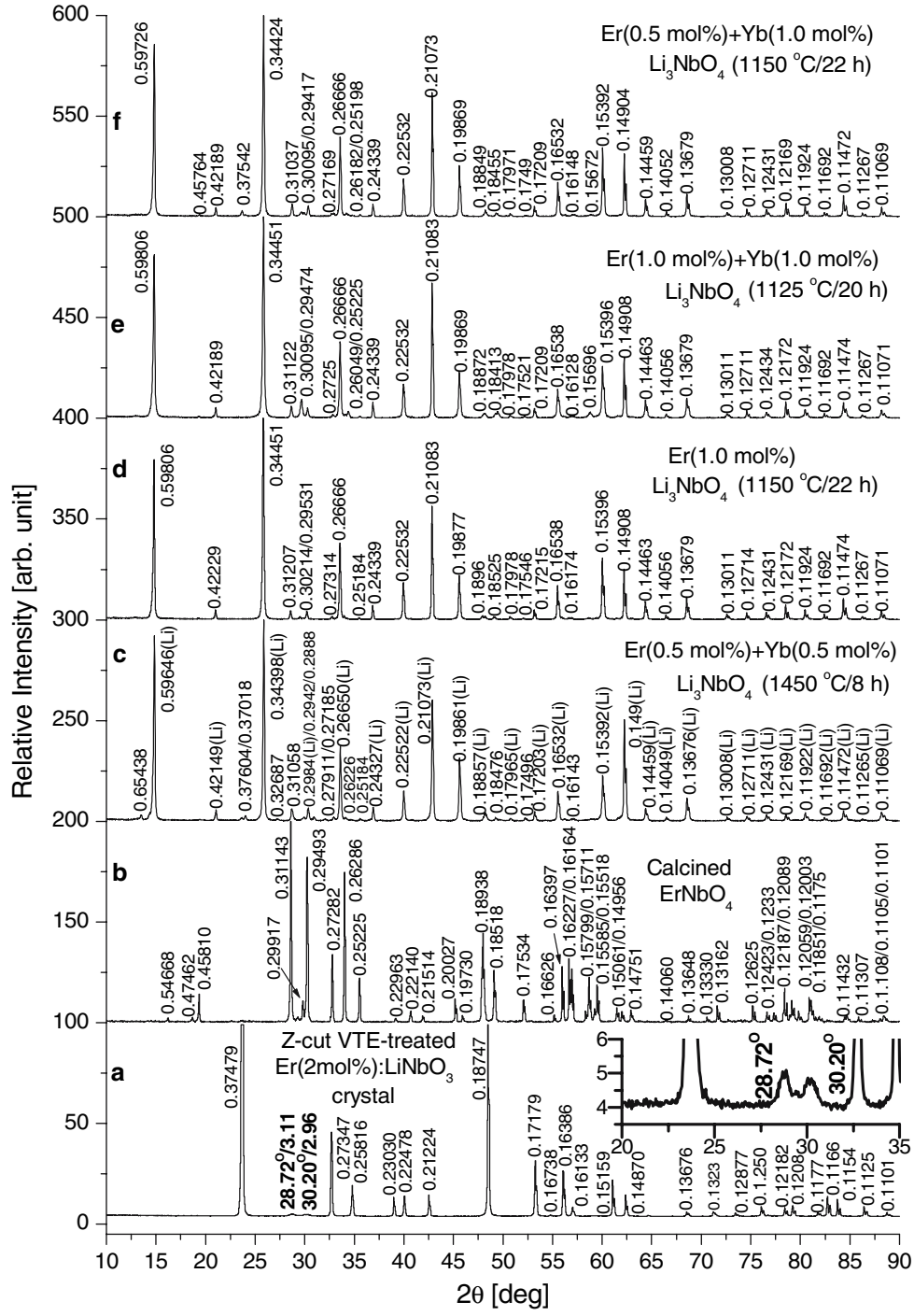

Fig. 1 Powder X-ray diffraction patterns of (**a**) VTE-treated Er(2.0 mol%):$LiNbO_3$ crystal (Z-cut), (**b**) thermally calcined $ErNbO_4$ powder, and (**c–f**) Li_3NbO_4 mixtures with different Er^{3+} and Yb^{3+} doping levels and calcination conditions. Data marked are the *d*-values corresponding to the $K_{\alpha 1}$ diffraction lines. The inset in pattern **a** shows an expanded view of two characteristic diffractions of $ErNbO_4$ phase around the 2 θ angles 30°

labeled c, d, e and f, respectively. The *d*-value is given in the unit of nanometer for each diffraction peak with respect to the $K_{\alpha 1}$ line.

At first, let us pay attention to the diffraction pattern of the VTE crystal. Two weak and broad additional reflexes (in comparison with the powder diffraction pattern of the corresponding as-grown Er:$LiNbO_3$ crystal) appear at around the 2θ angles of 30° and they are more clearly shown in inset in pattern a. The two peaks correspond to the strongest two reflexes in the diffraction pattern of the

pure $ErNbO_4$ as shown in the pattern b. They are the characteristic diffractions of the $ErNbO_4$ phase existing in the precipitates [8, 9]. Next, we discuss the crystalline phases contained in the calcined Er^{3+}-doped and Er^{3+}/Yb^{3+}-codoped mixtures. One can see from the patterns c–f in Fig. 1 that although the four rare-earth-doped mixtures were calcined under different temperatures and different durations, their diffraction patterns show little difference. Except that some individual reflexes with extremely weak intensity are discernible in one pattern and indiscernible in the other, and the relative diffraction intensity and *d*-value of individual reflex changes slightly from pattern to pattern, the patterns c–f are nearly the same as each other. Several powder diffraction files (PDFs) including the file 82–1198, 75–0902 and 75–0907, the source of which is given in Ref. [15], have provided diffraction data for trilithium niobate. It is found that all of the diffractions listed in these PDFs can find their counterparts in the patterns c–f. For convenience, all the reflexes listed in the PDF file are marked on pattern c with the symbol ''Li'' in the parentheses. One can see that these reflexes marked with the symbol ''Li'' dominate each diffraction pattern of c–f. It can be thus concluded that the trilithium niobate dominates all of the four rare-earth-doped mixtures. It can be further seen from the patterns c–f that each pattern still remains some relatively much weak reflexes that do not belong to the trilithium niobate phase. These remaining reflexes correspond well to those stronger diffractions of the $ErNbO_4$ phase. For example, the two reflexes with the *d*-values around 0.311 and 0.294 nm in the patterns c–f correspond to the strongest two diffractions in the pattern b. Moreover, most of the other remaining reflexes that include the diffractions with the *d*-values around 0.272, 0.262, 0.252, 0.185, 0.175 and 0.1615 nm in the patterns c-f can also find their counterparts in the pattern b. Therefore, it can be further concluded that the rare-earth-doped mixtures also contain the $ErNbO_4$ besides the trilithium niobate phase. Because the $YbNbO_4$ has the same crystal structure as the $ErNbO_4$, both thus have the similar powder X-ray diffraction patterns [3]. This means that the Er^{3+}/Yb^{3+}-codoped mixtures may also contain the $YbNbO_4$ phase.

Subsequently, let us return to the pattern a and examine if the VTE crystal also contains the Li_3NbO_4 phase in addition to the original $LiNbO_3$ and VTE-induced $ErNbO_4$ phases. If it is so, then the two strongest diffractions of the trilithium niobate, which have the *d*-values around 0.597 and 0.344 nm, should be discernible in pattern a because the two reflexes are located at the 2θ angles well separated from those of the diffraction peaks belonging to $LiNbO_3$ phase. However, such two reflexes cannot be resolved at all in the pattern a. This implies that the possibility that the VTE crystal contains the trilithium niobate phase is small.

In Fig. 1 the most remarkable diffraction feature is the large differences of the patterns between the VTE crystal, pure $ErNbO_4$ powder and rare-earth-doped mixtures. Based on the above-discussed crystalline phases contained in the VTE crystal and the rare-earth-doped mixtures, the differences between the patterns can be readily explained. For the VTE crystal, as demonstrated above, a large portion of $LiNbO_3$ phase and a little portion of $ErNbO_4$ phase are contained. For the doped mixtures, the phases $[RE^{3+}]NbO_4$ (RE^{3+} = Er or Yb) are present in each mixture only as the impurity and the trilithium niobate phase dominates each doped mixture. So, the X-ray patterns of the VTE crystal, pure $ErNbO_4$ powder and Er^{3+}(/Yb^{3+})-doped mixtures are mainly the contributions from the reflexes of the respective dominant phase $LiNbO_3$, $ErNbO_4$ and Li_3NbO_4. These three phases $LiNbO_3$, $ErNbO_4$ and Li_3NbO_4 possess different crystal structures. The corresponding space groups are R3C, I2 and $I\bar{4}3m$, respectively. The different crystal structures, of course, correspond to different X-ray diffraction patterns. So, the patterns show large differences.

The mechanism of phase transformation process in the doped mixtures can be simply described by an elevated-temperature-assisted solid-state chemical reaction: ($0.5x$ mol) Er_2O_3 + ($0.5y$ mol) Yb_2O_3 + [3 (50–$0.5x$–$0.5y$) mol] Li_2O + 50 mol Nb_2O_5 $\Leftrightarrow$ (x mol) $ErNbO_4$ + (y mol) $YbNbO_4$ + [(100–x–y) mol] Li_3NbO_4. Since all four rare-earth-doped mixtures show nearly same diffraction pattern and each pattern is essentially the overlap of the pattern of the Li_3NbO_4 with that of the $[RE^{3+}]NbO_4$ phase, therefore, the phase transformation in each mixture is essentially complete. This result implies that the two-phase or three-phase mixture can be readily prepared. The higher the calcination temperature, the faster the phase transformation procedure, and hence a shorter duration is needed. For example, at the calcination temperature 1450 °C, it needs only 8 h. At the lower temperature, the calcination duration required is also not very long. For example, at 1125 °C, it needs only 20 h.

Optical absorption and emission characteristics of Er^{3+} ions in the rare-earth-doped mixtures further confirm the above X-ray result that the Er^{3+} ions present in the mixtures in the form of the $ErNbO_4$ crystalline phase. Figure 2 shows the absorption spectra of the rare-earth-doped Li_3NbO_4 mixtures and the pure $ErNbO_4$ powder in the visible region. In our earlier paper [11] we have reported the visible absorption spectrum of the pure $ErNbO_4$ powder. The spectrum presented here is the re-measured one with improved quality. One can see that the visible spectra of the rare-earth-doped mixtures are not only essentially the same as each other, but also nearly identical to the spectrum of the $ErNbO_4$. Similar optical absorption feature is also observed for the $^4I_{15/2} \rightarrow {}^4I_{13/2}$ (~1.5 μm) transition as shown in Fig. 3.

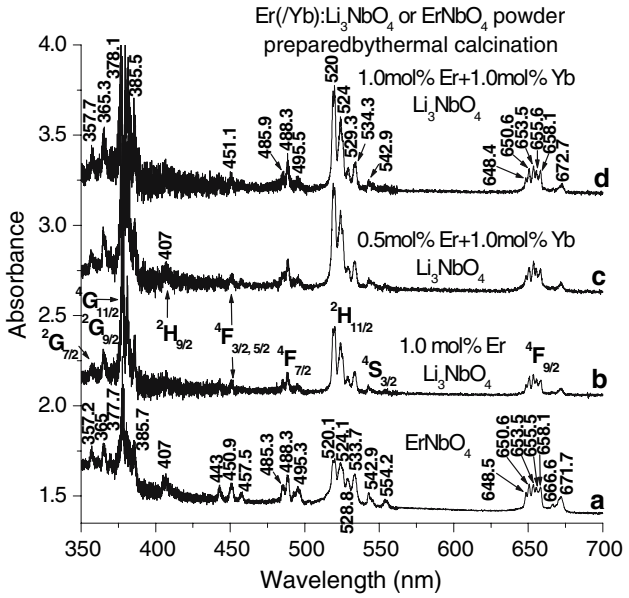

Fig. 2 Visible (350–700 nm) absorption spectra of (**a**) pure $ErNbO_4$, (**b**) Er(1.0 mol%):Li_3NbO_4, (**c**) Er(0.5 mol%)/Yb(1 mol%):Li_3NbO_4, and (**d**) Er(1 mol%)/Yb(1 mol%):Li_3NbO_4 powder. Signs and data indicated are the upper levels of the relevant absorption transitions and the peaking positions, respectively

Experimental results have shown that the fluorescence spectra of whether the rare-earth-doped Li_3NbO_4 mixtures or the pure $ErNbO_4$ powder are similar to their upconversion spectra. So, in Fig. 4 we only show the upconversion spectra of the doped mixtures and the pure $ErNbO_4$ powder. It can be seen that both green and red upconversion emission spectra of Er^{3+} ions in all rare-earth-doped

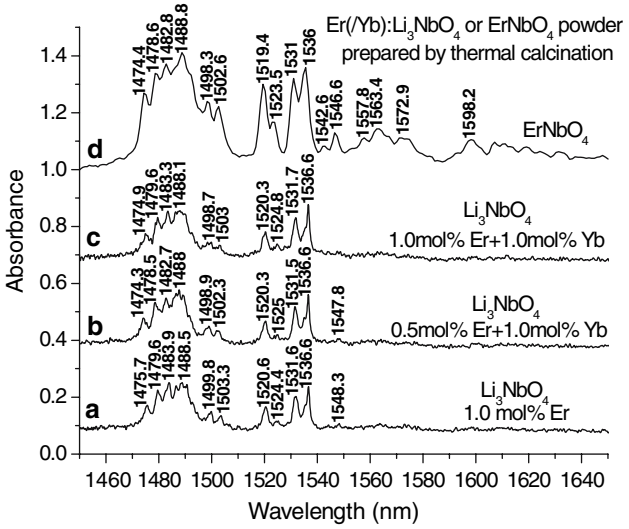

Fig. 3 Near infrared (1450–1650 nm) absorption ($^4I_{15/2} \rightarrow {}^4I_{13/2}$) spectra of (**a**) Er(1.0 mol%):Li_3NbO_4, (**b**) Er(0.5 mol%)/Yb(1 mol%):Li_3NbO_4, (**c**) Er(1 mol%)/Yb(1 mol%):Li_3NbO_4 and **d**: pure $ErNbO_4$ powder

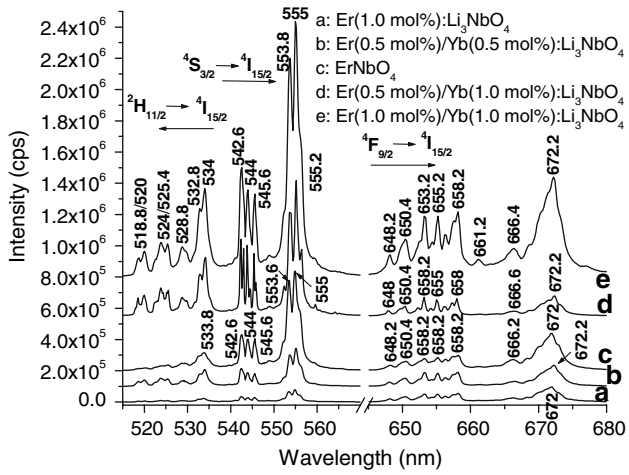

Fig. 4 Upconversion emission spectra of (**a**) Er(1.0 mol%):Li_3NbO_4, (**b**) Er(0.5 mol%)/Yb(0.5 mol%):Li_3NbO_4, (**c**) pure $ErNbO_4$, (**d**) Er(0.5 mol%)/Yb(1 mol%):Li_3NbO_4, and (**e**) Er(1 mol%)/Yb(1 mol%):Li_3NbO_4 powder. The involved transitions are indicated for the emission bands

Li_3NbO_4 powder show little differences in peaking position and spectral shape, and have a good corresponding relationship to the spectrum of the pure $ErNbO_4$ powder. On the other hand, it is shown in Fig. 4 that the upconversion emission intensity of Er^{3+} ion depends not only on the concentration of Er^{3+} ions in the sample, but also on the doping level of the Yb^{3+} ion. The higher the concentrations of Er^{3+} and Yb^{3+} ions are, the stronger the upconversion emission intensity is.

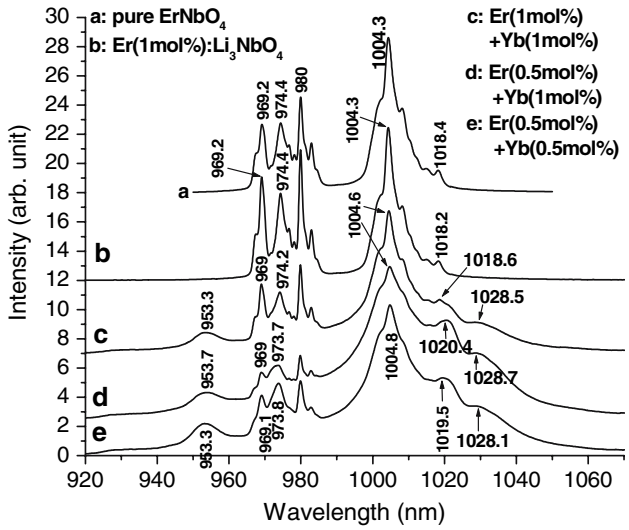

Fig. 5 Near infrared (920–1070 nm) emissions spectra of (**a**) pure $ErNbO_4$, (**b**) Er(1.0 mol%):Li_3NbO_4, (**c**) Er(1 mol%)/Yb(1 mol%):Li_3NbO_4, (**d**) Er(0.5 mol%)/Yb(1 mol%):Li_3NbO_4, and **e**: Er(0.5 mol%)/Yb(0.5 mol%):Li_3NbO_4 powder

Figure 5 shows the near infrared emission of the rare-earth-doped Li_3NbO_4 mixtures and pure $ErNbO_4$ powder in the 920–1070 nm region. For the case of the pure $ErNbO_4$ powder or the only Er-doped mixture, the recorded spectrum involves the pure Er^{3+} emission of $^4I_{11/2} \rightarrow {}^4I_{15/2}$. For the Er^{3+}/Yb^{3+}-codoped mixtures, the recorded spectra are the spectral overlap of the $^4I_{11/2} \rightarrow {}^4I_{15/2}$ emission of Er^{3+} with the $^2F_{5/2} \rightarrow {}^2F_{7/2}$ emission of Yb^{3+}. It can be seen that the spectrum of the only Er-doped Li_3NbO_4 mixture is essentially the same as that of the pure $ErNbO_4$ powder. As one proceeds from the only Er-doped mixture to the Er^{3+}/Yb^{3+}-codoped mixtures, the spectrum undergoes a certain extent of spectral alterations due to the spectral overlap of emissions from Er^{3+} and Yb^{3+}. The most noticeable spectral alterations take place around 953, 1020 and 1028 nm, where three additional bands arising from Yb^{3+} emissions are resolved. It is found that the spectral shape near the latter two bands shows definite Er^{3+} and Yb^{3+} doping level effect. At the higher doping level, 1.0 mol%, of Er^{3+}, the Er^{3+} emission near 1004 nm is relatively strong and the Yb^{3+} emissions near 1020 and 1030 nm are relatively weak. As a result, the Yb^{3+} emissions have a less effect on the spectral shape as shown by the spectrum c. At the lower doping level of Er^{3+} (0.5 mol%), however, the Er^{3+} emission near 1004 nm becomes relatively weak and the Yb^{3+} emissions become significant relatively and hence result in a relatively obvious spectral alteration. This can be seen from the spectra d and e. Moreover, it can be further seen from the spectra d and e that the emission intensity at 1020 and 1028 nm increases with a rise in Yb^{3+} doping level. Obviously, this feature is as expected. In addition, the emissions near 969 and 974 nm also display spectral alterations in relative intensity and peaking position. These spectral alterations are also the result from the overlap of the emissions of Er^{3+} and the codopant Yb^{3+}.

Figure 6 shows the 1.5 μm emissions ($^4I_{13/2} \rightarrow {}^4I_{15/2}$) of Er^{3+} ions in the rare-earth-doped mixtures and the raw material Er_2O_3 powder used for the preparation of the rare-earth-doped mixtures. For comparison, the spectrum of pure $ErNbO_4$ powder, which has been reported in our earlier paper [11], is also shown. As in the case of the emissions at 0.98 μm, the 1.5 μm emission spectrum of the only Er-doped Li_3NbO_4 mixture shows little difference with that of the pure $ErNbO_4$ powder in peaking position and spectral shape (see spectra labeled a and e). The influence of the Yb-codoping on the 1.5 μm emission is not significant. It affects only the relative emission intensity of individual peaks or bands. For example, the Yb-codoping causes enhancement of the band centered at 1490 nm, while does weakening of the emissions at 1609 nm with respect to the strongest emission at 1536 nm. The most remarkable feature in Fig. 6 is that the spectra of the pure $ErNbO_4$ and the doped mixtures are distinctly different from the spectrum of the Er_2O_3. This large spectral difference is due to the difference of the $ErNbO_4$ and Er_2O_3 phases in crystal structure. The space group of the $ErNbO_4$ as given above is I2, while that of the Er_2O_3 is T^5-$I2_13$ according to the powder diffraction file 08-0050.

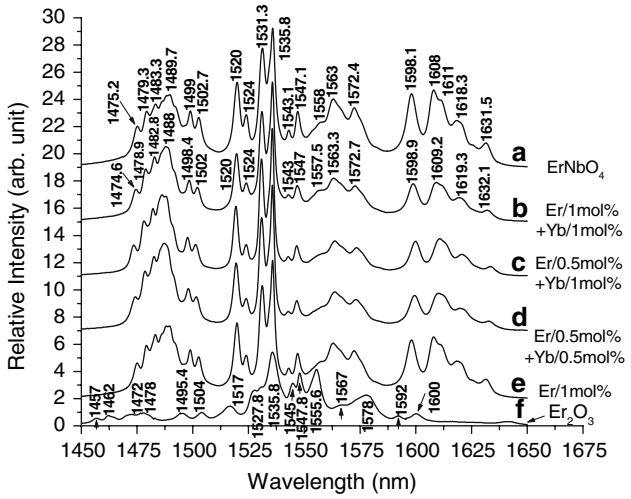

Fig. 6 Near infrared (1450–1650 nm) emission ($^4I_{13/2} \rightarrow {}^4I_{15/2}$) spectra of (**a**) pure $ErNbO_4$ powder, (**b**) Er(1 mol%)/Yb(1 mol%):-Li_3NbO_4, (**c**) Er(0.5 mol%)/Yb(1 mol%):Li_3NbO_4, (**d**) Er(0.5 mol%)/Yb(0.5 mol%):Li_3NbO_4, (**e**) Er(1.0 mol%):Li_3NbO_4 and (**f**) raw material Er_2O_3

The above optical studies have shown that the Er^{3+} ions in Er^{3+}(/Yb^{3+})-doped mixtures have the similar spectroscopic properties with those in the pure $ErNbO_4$ powder. This similarity implies that the Er^{3+} ions present in the doped mixtures as the $ErNbO_4$ crystalline phase and hence further confirm the conclusion drawn from the X-ray diffraction results.

Finally, we pay attention to the lifetimes at 1.5 μm of the Er^{3+} ions in the pure $ErNbO_4$ powder and the Er^{3+} (/Yb^{3+})-doped mixtures. Figure 7 shows the measured decays of the 1536 nm emission, which is the strongest emission of the $^4I_{13/2} \rightarrow {}^4I_{15/2}$ transition as shown in Fig. 6. For the pure $ErNbO_4$, the measured lifetime is similar to 2.0 ± 0.1 ms. In principle, the Er^{3+} ion in the Er^{3+}(/Yb^{3+})-doped mixtures should have the similar lifetime value to that in the pure $ErNbO_4$ powder. This is because all Er^{3+} ions in the doped mixtures present in the form of the $ErNbO_4$ crystalline phase. However, the measured lifetimes of the Er^{3+} ions in the 0.5/0.5, 0.5/1.0, 1.0/0.0 and 1.0 mol%/1.0 mol% Er^{3+}/Yb^{3+}-doped mixtures drop to 1.6 ± 0.1, 1.6 ± 0.1, 1.5 ± 0.1 and 1.4 ± 0.1 ms, respectively. The radiation trapping effect may be responsible for this discrepancy. The radiation trapping effect usually results in the lengthening of the Er^{3+} lifetime at 1.5 μm [16]. This effect is stronger in a medium with the high concentration of Er^{3+} ions. In connection to the Er-doped materials studied here, it is obvious that the pure $ErNbO_4$ powder has the highest concentration and the doped mixtures have the relatively much low concentration of the

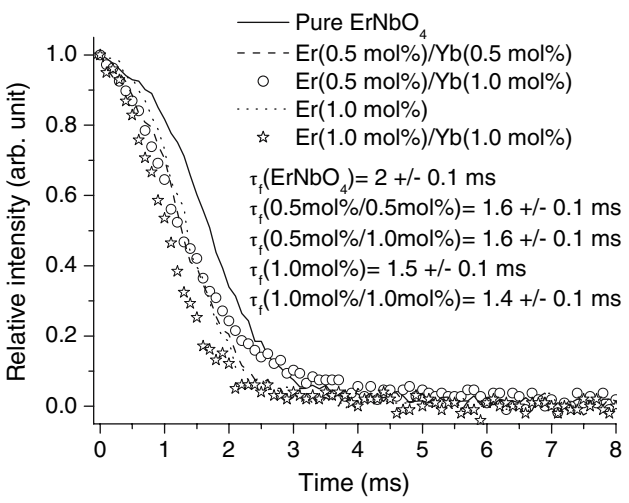

Fig. 7 The 1.5 μm fluorescence decays of $ErNbO_4$ (solid line), 0.5/0.5 (dashed line), 0.5/1.0 (open circle), 1.0/0.0 (dotted line) and 1.0/1.0 (five-star) mol%/mol% Er^{3+}/Yb^{3+}-doped Li_3NbO_4 powder. The τ_f values indicated are the measured lifetimes

active ions. So, the stronger radiation trapping effect in the pure $ErNbO_4$ powder may result in a certain extent of lengthening of the lifetime at 1.5 μm. Within the experimental errors, the lifetimes in the four $Er^{3+}(/Yb^{3+})$-doped mixtures are essentially identical (~1.5 ms) and do not show an obvious Er^{3+} or Yb^{3+} doping level effect. This behavior can be easily understood. Under the lower doping level of Er^{3+}, the radiation trapping effect is much weaker than the case of the pure $ErNbO_4$ and the lifetime should hold a constant. So, the behavior that the lifetimes in the mixtures doped with 0.5 mol% and 1.0 mol% do not show the obvious difference is comprehensive.

Conclusion

Singly Er^{3+}-doped and Er^{3+}/Yb^{3+} codoped Li_3NbO_4 powder were successfully prepared by thermally sintering the mixtures of Er_2O_3, Yb_2O_3, Li_2CO_3 and Nb_2O_5. X-ray diffraction studies show that the only Er^{3+}-doped mixture contains Li_3NbO_4 and $ErNbO_4$ two phases, and the Er^{3+}/Yb^{3+}-codoped mixtures may contain also the $YbNbO_4$ phase besides the Li_3NbO_4 and $ErNbO_4$ phases. X-ray diffraction results also show that the possibility that a highly Er-doped $LiNbO_3$ VTE crystal contains Li_3NbO_4 precipitates is small. The X-ray patterns of the mixtures doped with different concentrations of rare-earth ions show little difference each other, but display large differences with those patterns of the VTE Er:$LiNbO_3$ crystal and pure $ErNbO_4$ powder because three completely different phases Li_3NbO_4, $LiNbO_3$ and $ErNbO_4$ with different crystal structures dominate the doped mixtures, VTE crystal and pure $ErNbO_4$ powder, respectively.

Optical absorption and photoluminescence studies reveal that the Er^{3+} ions in the rare-earth-doped Li_3NbO_4 mixtures show similar absorption and emission characteristics with those ions in the pure $ErNbO_4$, indicating that the Er^{3+} ions present in these doped mixtures as the $ErNbO_4$ crystalline phase. This conclusion is consistent with that drawn from the X-ray diffraction results. The photoluminescence also reveal that the Yb^{3+} codpant can sensitize to enhance the green and red 980-nm-upconversion emissions of Er^{3+}. The emissions of Yb^{3+} ion overlap with those emissions of Er^{3+} ions in the 0.98 μm region and result in remarkable spectral alterations in this region. The extent of the spectral alterations depends on the doping level of Yb^{3+}. In addition, Yb-codoping also causes the alterations of relative absorbance and relative emission intensity of individual peaks or bands in the 1.5 μm region. On the other hand, the Yb-codoping hardly affects the absorption or emission peaking position in both visible and 1.5 μm regions. The influence of the Yb^{3+} codopant on the lifetime of Er^{3+} ion at 1.5 μm is also small. The measured lifetimes at 1.5 μm of Er^{3+} ions in the singly Er^{3+}-doped and Er^{3+}/Yb^{3+}-codoped mixtures are nearly same within the experimental errors and have a value similar to 1.5 ms. For the pure $ErNbO_4$ powder, however, the lifetime is prolonged to ~2 ms probably due to the radiation trapping effect.

Acknowledgement This work was supported by National Natural Science Foundation of China under Project no. 60577012.

References

1. Gill DM, McCaughan L, Wright JC (1996) Phys Rev B 53:2334
2. Zhang DL, Chen XJ, Wang YF, Zhu DS, Wu B, Lan GX (2002) J Phys Chem Solids 63:345
3. Zhang DL, Wong WH, Pun EYB (2004) J Phys Condens Matter 16:7793
4. Zhang DL, Wang DC, Pun EYB (2005) J Appl Phys 97:103524
5. Zhang DL, Wong WH, Pun EYB (2004) J Crystal Growth 271:184
6. Zhang DL, Pun E YB, Chen XJ, Wang Y, Jin YH, Zhu DS, Wu ZK (2002) J Appl Phys 91:4014
7. Zhang DL, Pun EYB (2003) J Appl Phys 93:3141
8. Zhang DL, Lan GX, Chen XJ, Zhu DS (2002) Appl Phys A: Mater Sci Process 74:265
9. Zhang DL, Pun EYB (2003) J Appl Phys 94:1178
10. Zhang DL, Pun EYB (2004) J Alloys Compounds 370:315
11. Zhang DL, Wang YF, Yu YZ, Chen CH, Yao JQ, Pun EYB (2004) Optical Materials 25:379
12. Zhang DL, Wang DC, Wang YF, Pun EYB (2004) Physica Status Solidi A 201:2334
13. Reisman A, Holtzberg F (1958) J Am Chem Soc 80:6505
14. Shishido T, Suzuki H, Ukei K, Hibiya T, Fukuda T (1996) J Alloys Compounds 234:256
15. Powder Diffraction File (PDF) Card No. 82–1198, provided by Joint Committee on Powder Diffraction Standards (JCPDS)
16. Muñoz JA, Herreros B, Lifante G, Cussó F (1998) Phys Status Solidi A 168:525